

Structure and magnetism of cobalt at high pressure and low temperatureR. Torchio,^{1,2} C. Marini,^{1,3} Y. O. Kvashnin,^{1,4} I. Kantor,¹ O. Mathon,¹ G. Garbarino,¹
C. Meneghini,⁵ S. Anzellini,^{2,6} F. Occelli,² P. Bruno,¹ A. Dewaele,² and S. Pascarelli¹¹*ESRF-The European Synchrotron 71, Avenue des Martyrs, Grenoble, France*²*CEA, DAM, DIF, F-91297 Arpajon, France*³*ALBA Synchrotron/CELLS, Cerdanyola del Valles, E-08290, Spain*⁴*Department of Physics and Astronomy, Division of Materials Theory, Uppsala University, Box 516, SE-75120, Sweden*⁵*Dipartimento di Scienze, University ROMA TRE, via della Vasca Navale 84, Rome, Italy*⁶*Diamond Light Source Ltd., Diamond House, Harwell Science and Innovation Campus, Didcot, OX11 0DE, United Kingdom*

(Received 29 July 2015; revised manuscript received 16 March 2016; published 22 July 2016)

The magnetic and structural properties of cobalt were investigated under high pressure (160 GPa) and low temperature (50 K), by synchrotron K-edge x-ray magnetic circular dichroism and x-ray diffraction. A quasihydrostatic equation of state was measured up to 160 GPa. We found that uniaxial stress plays a role in the hexagonal close packed-face centered cubic (hcp-fcc) structural transition pressure. Also, our data provide the first experimental evidence that changes of the c/a ratio pressure derivative are related to the magnetic behavior. The complete extinction of ferromagnetism is observed above 130 GPa in a mixed hcp-fcc phase with no recovery upon cooling to 50 K, indicating that cobalt at 150 GPa is very likely nonmagnetic, i.e., characterized by zero local spin polarization. Density functional theory calculations point out that the K-edge x-ray magnetic circular dichroism (XMCD) signal is related to the $4p$ orbital moment rather than to the total spin moment and allow us to get a deeper insight into the K-edge XMCD measurements interpretation. The combination of novel theoretical results and experimental outputs provides a detailed scenario of the structural and magnetic properties of cobalt at these extreme conditions answering some previously unsolved issues.

DOI: [10.1103/PhysRevB.94.024429](https://doi.org/10.1103/PhysRevB.94.024429)**I. INTRODUCTION**

Cobalt, situated at the center of the magnetic $3d$ transition metal series, plays a crucial role in the systematic understanding of magnetic $3d$ elements. It is the 30th most abundant element on Earth and comprises approximately 0.0025% of the Earth's crust. Cobalt is used in high temperature alloys of the superalloy type because of its resistance when heated up to fairly high temperatures. It also has good work-hardening characteristics, which contribute to the interest in its use in wear alloys. Cobalt-based materials are attractive for their chemical, magnetic, and electronic properties with potential applications in such fields as magnetic data storage and catalysis [1–3]. Following iron in the periodic table, cobalt plays also an important role in defining the properties of the Earth's core, which is believed to be composed of iron-dominated alloys with perhaps Co or Ni as minor components. Understanding the behavior of Co under extreme pressure and temperature conditions represents thus an important, interdisciplinary issue.

In 2000 Yoo and coworkers [4] reported the first evidence of a pressure-induced hexagonal close packed-face centered cubic (hcp-fcc) transition in cobalt, characterized by no change in volume and a broad coexistence range (about 100–150 GPa). Such a large interval of coexistence was attributed to the nonhydrostatic conditions of the sample and to the small energy difference between the two phases [5]. Theoretical calculations predict the high-pressure fcc structure, to become energetically favorable with respect to the hcp around 100 GPa [6–8] in agreement with the observed experimental onset; however, experimental findings depict a relatively large spread of the hcp-fcc transition onset with lowest values found at 70–80 GPa [9] and highest values at ≈ 145 GPa [8]. The calculated volume change is 1–3% [6,7]

and the hcp-fcc structural transition is classified as a first-order one [7]. Later on, Antonangeli and coworkers [10] measured a quasihydrostatic equation of state (EoS) of hcp cobalt up to 90 GPa pointing out an inversion in the pressure evolution of the axial c/a ratio of the hcp phase around 75 GPa, in the same pressure range at which anomalies in the elastic and vibrational properties occur [11,12]. Measurements of the Raman active transverse optical phonon mode, which can be related to the shear elastic constant, show a change in slope of the E_{2g} mode Gruneisen parameter near 60 GPa [11]. The measurements of aggregate elastic constants by both impulsive stimulated light scattering [11] and inelastic x-ray scattering [10] show an even more anomalous behavior, with the shear modulus softening in the range of 70–100 GPa. This is best seen in deviations from an expected linear density dependence of longitudinal (v_L) and transverse (v_T) acoustic velocities with a sublinear relation and even softening in v_L and v_T . First-principles calculations [6,8,10] demonstrate that these structural and elastic anomalies coincide with the onset of the loss of ferromagnetism in the hcp Co phase, thus suggesting a magnetoelastic coupling between acoustic phonons and spin-wave branches (magnons) as the driving factor. However, a direct experimental evidence of the coupling between magnetic, structural and elastic properties is still lacking. Another recent theoretical study shows that at around 80 GPa there is an electronic topological transition taking place in hcp Co [13]. This transition drastically modifies the density of states at the Fermi level and is suggested to be the reason for the observed anomalies in both magnetic and elastic properties.

Several calculations in the literature, mainly based on the density functional theory (DFT), describe the magnetic behavior of both compressed hcp and fcc Co phases [6–10,14–18]. The calculated magnetic moment of hcp and fcc

cobalt decreases with increasing pressure. This is qualitatively understood in the framework of the Stoner-Wohlfarth model: compression leads to the broadening of the bands resulting in a lower density of states at the Fermi level such that the magnetic state stability condition given by the Stoner criterion is no longer met. There is a general agreement [6–10,14,17,18], even though with some exceptions (Ref. [16] and Ref. [14] in the GGA+U case), on the qualitative trend of the moments suppression and on the fact that the fcc structure is theoretically predicted to lose its magnetic moment at lower compression with respect to the hcp, although there is some uncertainty (20%) in the values of the critical pressure for magnetization extinction for both phases. The pressure dependence of the magnetic moment in both phases shows a slow and almost linear behavior up to 60–80 GPa. This is followed by a more rapid decrease until total suppression at 70–120 and 90–180 GPa for the fcc and hcp phase, respectively (see Fig. 3.6 in Ref. [19]).

The magnetic response to compression for cobalt has been experimentally investigated by K-edge x-ray circularly polarized absorption, which simultaneously brings magnetic and structural information through x-ray magnetic circular dichroism (XMCD) and x-ray absorption near edge spectroscopy (XANES) [17,20–22]. The cobalt K-edge XMCD signal starts decreasing immediately and continuously upon pressure application, long before the onset of the structural transition. However, some controversial results emerged from the most recent works. In our previous study [17] we observed a zero XMCD signal at 120 ± 10 GPa, pointing out the complete loss of ferromagnetism, and the analysis of the XANES spectra indicated that this occurred in a mixed hcp-fcc phase and not in the pure fcc phase as previously suggested [20]. On the other hand, Ishimatsu *et al.* [22] found a residual (10%) XMCD signal from 130 up to 170 GPa, in the fcc stability range (as seen by XANES). Using field-dependent measurements (with maximum field induction of 0.6 Tesla), the authors suggested this residual magnetic signal to be the fingerprint of a transition to a fcc paramagnetic state.

The literature findings give rise to a complex panorama with open questions and relatively spread results that stimulates us to further explore the high-pressure structural and magnetic behavior of Co and their correlation. In this work we exploited polarized absorption (K-edge XMCD) to probe the magnetic behavior of pure Co at high pressure and low temperature, in order to disentangle the elementary magnetic moment suppression from Curie temperature effects. The coupling of Mbar pressures to low temperature is quite challenging and in our previous experiment carried out at room temperature, this had not been possible [17]. Moreover, in that work we had estimated the hcp/fcc phase fraction across the structural transition from the XANES data. The accuracy in the determination of the hcp/fcc phase fraction relies on very small differences in the simulated XANES profiles of the two structures, and therefore is less accurate than using high quality XRD patterns. In the present work, we used high pressure x-ray diffraction (XRD) to obtain a quasihydrostatic EoS up to 160 GPa—being an original achievement of this work—and to perform simultaneous (room temperature) XRD and XMCD measurements allowing to trace the interrelationship of the structural and magnetic transition with higher accuracy, while

furnishing a direct measurement of volume compression. Coupling high-pressure polarized absorption, a chemical selective magnetic probe, and XRD thus provide a detailed understanding of Co magnetic and structural properties from a local and crystallographic perspective. In particular, we have addressed two open questions that previous investigations, including our own, had left unanswered: (1) what is the long-range structure of cobalt in the nonferromagnetic state? (2) Does the nonferromagnetic state reflect a paramagnetic phase with randomly oriented local magnetic moments?

Finally, in our previous work on pure Ni [23], we had shown by means of DFT calculations that the behavior of the K-edge XMCD signal under compression follows that of the *p*-projected orbital moment rather than that of the total spin moment. We present here analogous calculations for the more complex Co case and a simple theoretical model, allowing us to get a deeper insight into the interpretation of the K-edge XMCD measurements.

II. EXPERIMENTAL METHODS

The quasihydrostatic EoS has been obtained using synchrotron radiation high-pressure x-ray diffraction. A grain of high-purity polycrystalline powder cobalt from a Goodfellow was loaded in a Le Toullec [24] type diamond anvil cell (DAC), equipped with beveled 75×300 culets diamonds, together with tungsten as pressure calibrator [25] and neon as transmitting medium. Angle dispersive diffraction patterns were collected up to around 160 GPa on the ID27 beamline [26] at the European Synchrotron Radiation Facility (ESRF) using a monochromatic x-ray beam ($\lambda = 0.3738$ Å).

For the coupled XMCD-XRD run, a high-purity polycrystalline Co powder (from Goodfellow) was loaded in an amagnetic DAC equipped with beveled 70×300 culets diamonds. No pressure transmitting medium was used in this case. Powder loading, covering the entire hole, is more suited for absorption measurements since a high degree of sample homogeneity is required in this kind of experiment, of course, at the expenses of less hydrostatic conditions. For each pressure, the volume compression was measured from the XRD pattern collected on the beamline ID27 according to the procedure described in Ref. [23]. XANES and XMCD signals were recorded at the energy dispersive x-ray absorption spectroscopy beamline ID24 [27] (ESRF) at the Co K edge ($E_0 = 7709$ eV) using a highly focused beam ($5 \mu\text{m}$ full width at half maximum). The field induction was 0.7 Tesla.

In this run, XAS spectra and XRD patterns were collected up to a volume compression of $V/V_0 = 0.695$, corresponding to a pressure of around 150 GPa. The cell was then cooled down to 50 K using a dedicated cryostat to acquire low-temperature XMCD spectra.

III. RESULTS AND DISCUSSION

A. EoS, hcp-fcc transition, and *c/a* behavior

In Fig. 1 we report the compression data obtained in quasihydrostatic conditions on the Co grain (red circles), compared to data from Dewaele and coworkers [28] (black squares), EoS from Antonangeli *et al.* [10] and Yoo *et al.* [4]. For the fit to the Vinet function [29], we merged our data

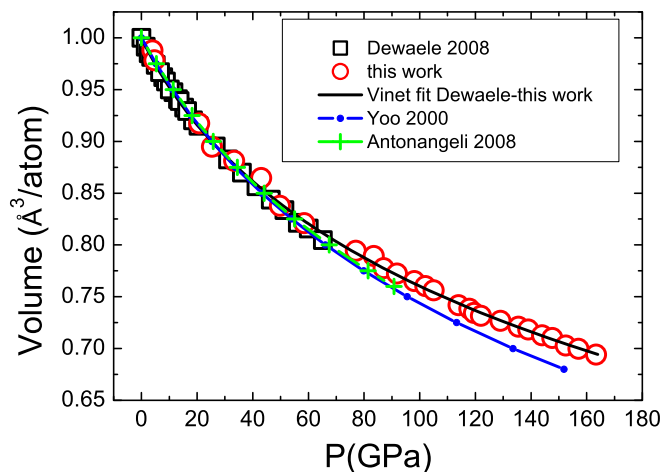


FIG. 1. Compression data on a hcp Co grain measured in quasi-hydrostatic conditions (empty red circles) and fit to a Vinet EoS (black line) of these data merged to data from Ref. [28] (empty black squares); previous EoS from Refs. [4] and [10] are shown for comparison.

with lower-pressure data from Ref. [28], acquired on the same kind of sample, also in quasi-hydrostatic conditions and with a pressure gauge whose calibration agrees with the present one [25]; the fit is shown in black line. The fit parameters for the EoS are reported in Table I in comparison to results from the literature. No structural transition was observed up to 164 GPa, indicating that the hcp-fcc phase transition observed in Yoo *et al.* [4] in the 100–150 GPa range is related to the nonhydrostatic conditions and to the metastability of the two phases. The hcp and fcc structures differ only in their stacking sequence of the planes, so the transition requires relatively small atomic displacements and thus occurs martensitically. In martensitic transitions, and in general in transitions characterized by a small change in volume, the presence of uniaxial stress given by nonhydrostatic conditions has a strong effect on the transition pressure, lowering the transition onset pressure and widening the transition pressure width. This was observed, for example, in Ti [30,31].

In fact, in our nonhydrostatic run, the fcc phase appeared and coexisted with the hcp phase for compression from $V/V_0 = 0.763$ to 0.694 (Fig. 2), the maximum compression reached. In this run, we chose to evaluate the pressure using XRD volume data and the EoS measured in this study and in Yoo *et al.* [4]: $P = (P_{\text{This study}} + P_{\text{Yoo}})/2$. The maximum error on the pressure, given by the EoS variation, amounts to 10%. At the transition, a volume change of $\Delta V \approx 0.14 \text{ \AA}^3/\text{atom}$

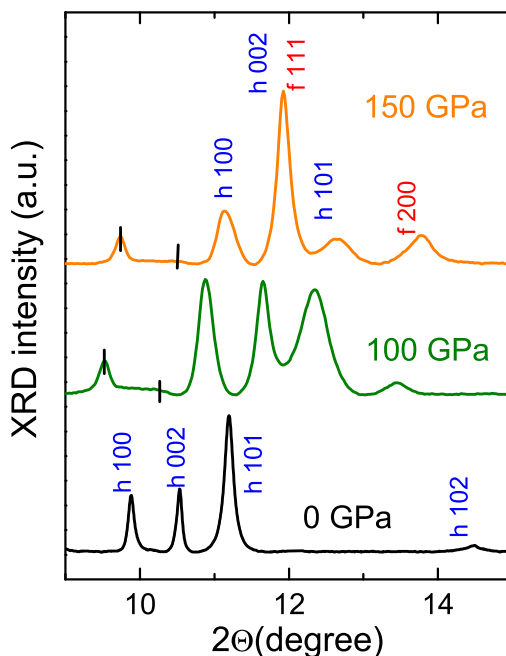


FIG. 2. Selection of XRD patterns acquired at room temperature during the nonhydrostatic combined XRD-XMCD run. Reflections from the hcp and fcc phases are indicated as h and f, respectively. Diffraction peaks from the Co fcc phase appear around 90 GPa; small vertical lines indicate reflections from the Re gasket.

(1.25%) was observed (Fig. 3), in agreement with theoretical predictions [6,7] and differently from Ref. [4] where no volume change was observed.

The analysis of the relative intensities of hcp and fcc reflections allows evaluating the hcp/fcc phase fraction which results around 0.5 at the maximum compression reached; the value obtained at pressures of 120 GPa is around 0.7, quite in agreement with the estimation of 0.6 previously deduced from XANES simulations [17]. The diffraction rings showed no significant presence of texture of the sample, therefore this was not taken into account. We estimate that the error on the hcp/fcc phase fraction is around 10%. The extrapolation of the XRD analysis suggests that the hcp and fcc phases may coexist up to 200 GPa, which is in agreement with Fig. 1 of Ref. [4], where the (100) reflection from the hcp phase is still visible in the 202 GPa pattern. In Fig. 4 we report the hcp and fcc phase domains as a function of pressure and pressurizing conditions found in this study and comparison with results reported in the literature.

TABLE I. Parameters of the Vinet EOS obtained by least-squares fit of the experimental compression data of hcp Co: V_0 denotes equilibrium volume, B_0 is the bulk modulus, and B'_0 is its pressure derivative. P and PTM stand for pressure and pressure transmitting medium, respectively. EoS reported in the literature are shown for comparison.

	EOS fit	Pressure gauge	$V_0(\text{\AA}^3/\text{atom})$	$B_0(\text{GPa})$	B'_0	P range	PTM
This work	Vinet	W EoS [25]	11.09(7)	186(8)	5.1(4)	0–160	Ne
Dewaele	Vinet	Ruby [25]	11.096	190.5(2.9)	4.38(18)	0–65	He
Antonangeli	third-order Birch Murnaghan	Ruby [32], Pt EoS [28]		199(6)	3.6(0.2)	0–90	Ne
Yoo	third-order Birch Murnaghan	Pt [33] and Ta EoS [34]	11.24	199	3.6	0–202	Ar or NaCl

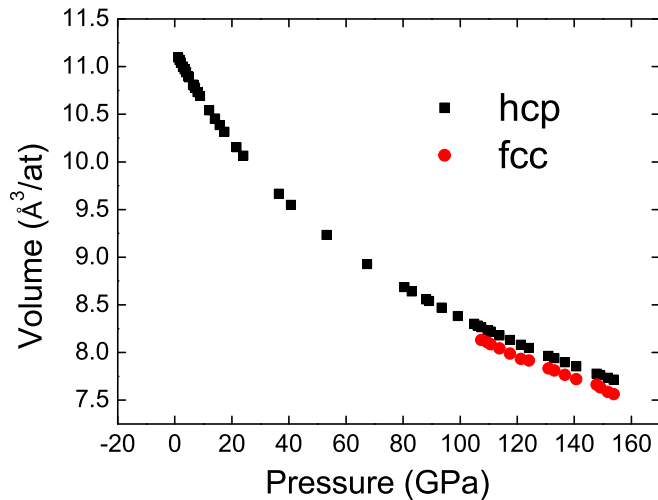


FIG. 3. Volume compression of hcp and fcc Co.

With increasing pressure, the axial ratio c/a decreases until the volume compression of $V/V_0 \approx 0.76$, where it reaches its minimum and then starts increasing again. This inversion in the pressure derivative of the axial ratio was previously observed by Antonangeli *et al.* [10]. In Fig. 5 we compare the c/a ratio behavior of cobalt measured in quasihydrostatic and nonhydrostatic conditions as a function of volume compression. Apart from a shift in the absolute value of around 0.5%, they depict quite similar behaviors as a function of compression. At compressions of $V/V_0 \approx 0.725$ the c/a ratio stabilizes around the value of 1.621, in agreement with theoretical calculations [10,35]. A different result was found by Yoo *et al.* [4], where the c/a ratio increased up to 1.65 (Fig. 4), clearly indicating a deviation from the closed packed symmetry.

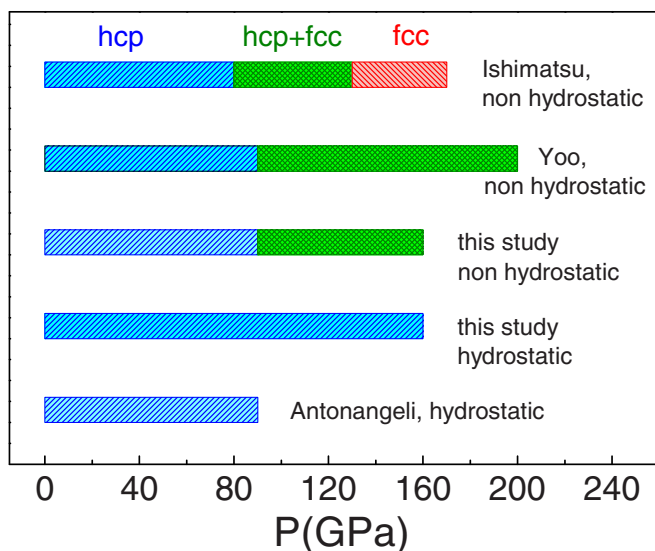
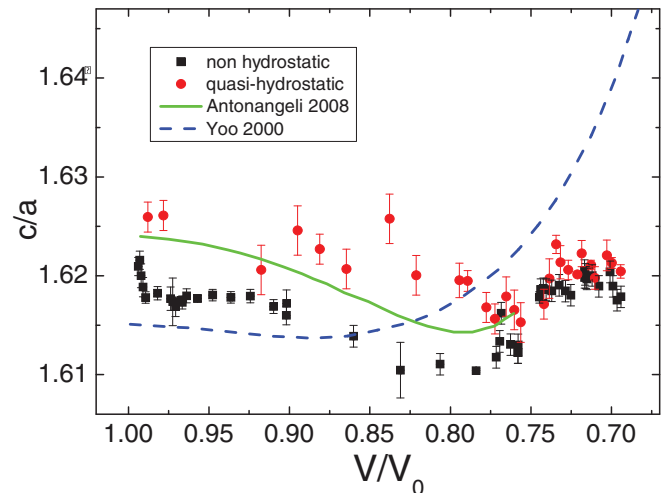


FIG. 4. Schematic overview of hcp and fcc Co phases domains found in this study and in previous literature as a function of pressure (room temperature) and hydrostatic conditions.

FIG. 5. c/a value as a function of compression for the Co grain compressed in Ne (quasihydrostatic run, red circles) and Co powder (nonhydrostatic run, black squares) and comparison to previous trend reported in Ref. [10] (green line) and Ref. [4] (blue dashed line).

In the quasihydrostatic run the inversion in the pressure evolution of the axial ratio occurs around $V/V_0 = 0.76$, while in the nonhydrostatic run at slightly lower compressions around $V/V_0 = 0.78$, similarly as in Antonangeli *et al.* [10]. The different compression found in our hydrostatic run and in Ref. [10], also hydrostatic, could be due to a different microstructure of the sample or to different hydrostatic conditions. The sample in Ref. [10] was a powder initially precompressed to eliminate a metastable fcc phase. Most importantly, the present results demonstrate that the c/a pressure derivative inversion is not correlated to the occurrence of the hcp-fcc structural transition, since we did not observe the transition in the quasihydrostatic run.

B. Extinction of ferromagnetism and link to the c/a behavior

During compression, the K-edge XMCD signal is progressively suppressed (Fig. 6) following a trend already encountered in previous studies (Fig. 6, central panel) [17,20–22]: the signal decreases linearly and continuously up to around 80 GPa; above 80 GPa it undergoes a stronger inflection, in correspondence to the appearance of the fcc phase. The total disappearance is observed above 130 GPa, indicating the loss of ferromagnetic order. Differently from the work of Ishimatsu *et al.* [22], we find no residual signal in the 130–150 pressure range. We notice that the noise in our data is of the same order of magnitude as in Ref. [22], therefore such a residual signal could not be hidden. For each XMCD pressure point the cell was brought to ID27 to acquire diffraction. A selection of diffraction patterns is shown in Fig. 2. Most importantly, combining XMCD and XRD data we are able to unambiguously demonstrate the extinction of the K edge XMCD signal occurring in a mixed hcp-fcc phase. This implies that the remaining hcp phase is also nonferromagnetic. After the pressure in the cell reached 150 GPa, the DAC was cooled down to 50 K. The external pressure drive allowed us to compensate for the decreasing

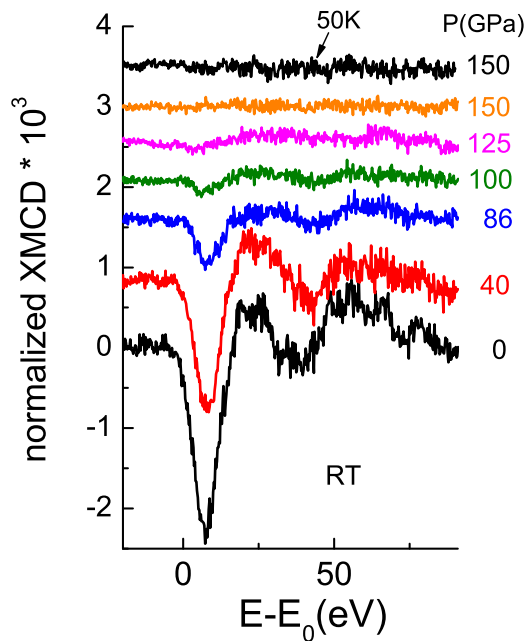


FIG. 6. XMCD evolution as a function of pressure: all spectra are acquired at room temperature (RT) except the one on the top (black) which was acquired at 150 GPa and 50 K.

helium volume in the membrane capillary, assuring that the pressure in the sample chamber was kept constant. As a double check, we estimated the compression from the shift of the first EXAFS oscillation, as described in previous works [17]; the obtained compression $V = 0.692$ is in agreement with the compression measured from XRD before cooling. No relevant changes were observed at low temperature, in particular, no reappearance of the XMCD signal was observed (Fig. 6). Under compression, both the magnetization and the Curie temperature are supposed to vary. The Curie temperature (T_c) in Co is 1400 K at ambient pressure and a slight increase with pressure was reported up to 25 GPa [36]. Unfortunately, neither theoretical nor experimental data of the cobalt T_c evolution are available at higher pressures. Assuming that the T_c does not fall below 50 K at 130 GPa, our result indicates that the compression of cobalt to 150 GPa leads to a nonmagnetic state—characterized by zero elementary moment—and not to a paramagnetic state above the T_c .

Comparing to structural data (Fig. 7) we observe that the evolution of the XMCD signal and that of the c/a ratio are correlated: the inversion in the pressure derivative of the axial ratio c/a occurs in correspondence to the beginning of the XMCD faster drop. On the other hand, the c/a behavior is not related to the structural hcp/fcc transition as we have seen from the quasihydrostatic run, where no structural transition occurred. Hence, the combination of XMCD and XRD measurements demonstrates that the peculiar behavior with pressure of the c/a ratio is related to changes in the magnetic behavior and not to structural changes.

C. Theoretical interpretation of the measured magnetism

A set of DFT calculations was carried out using the Wien2K [37] software package. A GGA-type [38] exchange-

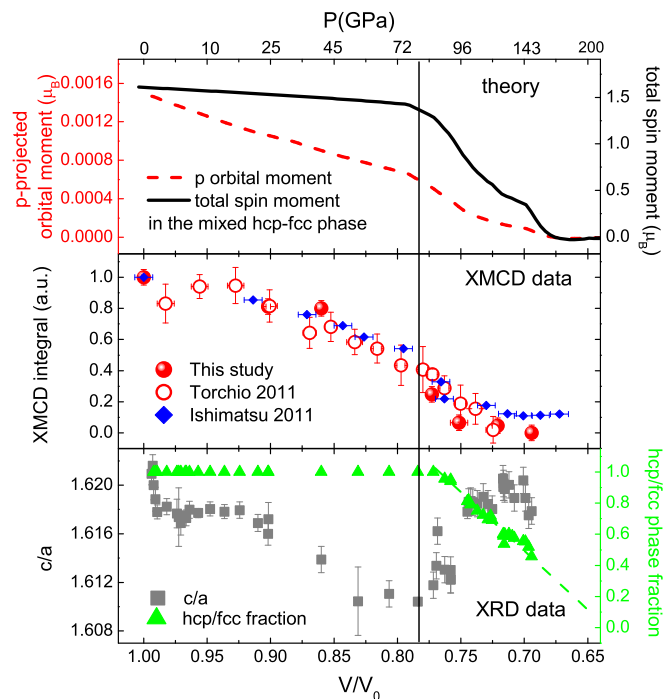


FIG. 7. Top panel: Calculated total spin moment and the p -projected orbital moment in the mixed hcp-fcc phase, according to the fraction found from XRD, and assuming that the magnetization in both phases is aligned parallel to each other. Central panel: K-edge XMCD integrals from the present work (full circles) and the previous study (empty circles [17]) and data from Ishimatsu *et al.* [22]. Bottom panel: hcp/fcc phase fraction obtained from the XRD analysis and inversion of c/a ratio pressure derivative as a function of compression in this run.

correlation potential was employed. We have investigated various contributions of the total magnetization and tried to relate XMCD results with the outcome of first-principles calculations. Following the approach by Antonangeli *et al.* [12], the c/a ratio was obtained as the value that minimizes the total energy for each value of the volume of the cell. Computational details are the same as were used in Ref. [23]. Opposite to the case of Ni, the d -orbital moment of hcp Co is almost a factor two underestimated in the conventional DFT [39,40]. In order to improve this, we applied the orbital-polarization correction (OP) to the d -states. The results obtained with GGA and GGA+OP schemes for various unit cell compressions are shown in Fig. 8.

It is seen that whereas spin moments are rather insensitive to the added OP correction, orbital moments are indeed increased, providing results that are in better agreement with ambient pressure experimental values [4,28]. However, both GGA and GGA+OP predict the collapse of the magnetic moment at the same volume (around $0.75 V_0$ for the hcp phase). This is not surprising since the form of the OP correction is such that the enhancement of the orbital moment is proportional to the magnitude of the orbital moment itself. Hence, when the latter collapses upon compression, the OP correction shrinks to zero as well and, therefore, does not lead to any modification of the phase diagram. The pressure dependence of the magnetic moments dramatically changes at $0.8 V_0$ (≈ 80 GPa) in both

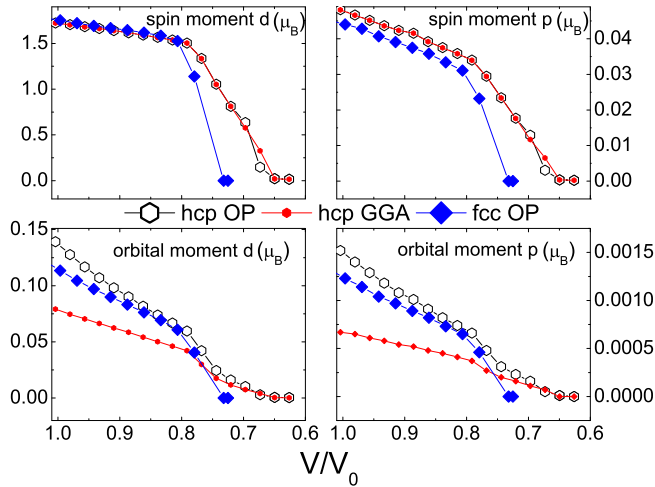


FIG. 8. Calculated spin and orbital components of l -projected magnetic moments in hcp and fcc Co as a function of compression. Note that absolute values are plotted; $\langle S \rangle_p$ is antiparallel to $\langle S \rangle_d$. V_0 is the calculated equilibrium volume for a given crystal structure

crystal structures. At such compressions the magnetic splitting is not sufficient to keep the entire majority-band occupied. As a result, spin-up states start to cross the Fermi level and this makes the magnetic moment more sensitive to pressure (i.e., the system becomes a weak ferromagnet) [13]. We witness that in both OP and non-OP cases, the quenching of the orbital moment upon compression is much faster than that of the spin moment. At first sight, this result might look counterintuitive. However, it can be understood on the basis of a simple quantum mechanical picture. If spin-orbit coupling (SOC) is added as a second-order perturbation to the $3d$ states, the produced orbital moment ($\langle L \rangle_d$) is proportional to $(\xi/\Delta_{cf}) \cdot \langle S \rangle_d$ where ξ is the SOC constant (≈ 0.05 eV) and Δ_{cf} is the crystal field splitting (see, e.g., Ref. [41], p. 307). ξ is an atomic parameter and can be expected not to change much with pressure, while Δ_{cf} tends to increase. This implies that orbital moment should attenuate faster than the spin moment upon compression. In metallic systems, there is no direct relationship between spin and orbital moments. The latter results from an interplay between crystal structure, band filling, and spin-orbit coupling. Moreover, it is known that, for instance, dynamical correlation effects influence spin and orbital magnetism in different ways [42]. Thus, we again emphasize that their analysis has to be done separately.

Let's now consider a simplified model in which at each volume there is a random mixture of hcp and fcc phases. Furthermore, we assume that all Co magnetic moments are aligned parallel to each other, thus the total magnetization is a weighed sum of the magnetic moments in the two phases. The full and dashed lines in the top panel of Fig. 6 represent the calculated total spin and $4p$ orbital moment of the mixed hcp-fcc phase weighted to the fraction found from XRD. In the central panel, we plot XMCD data for comparison. At $V/V_0 = 0.69$, the highest compression probed experimentally, the XMCD signal is zero within our resolution, the hcp/fcc fraction is 50% and the theoretical total spin and p orbital

moment for the mixed phase are 16% and 4% of their initial value, respectively. Therefore, the comparison of experimental and theoretical results supports a faster suppression of the magnetization with respect to the structural transition, i.e., the nonmagnetic state should be reached before cobalt is totally in the fcc phase.

Like it was found for the nickel case [23], the relative decrease of the XMCD integral is comparable to that of the p -projected orbital moment and not to that of the total spin moment. At $V/V_0 = 0.69$ the theoretical p -orbital moment is only 4% of its initial value, thus comparable with our XMCD experimental resolution, whereas the theoretical total spin moment is still 16%. Therefore, we cannot in principle exclude residual ferromagnetism at this compression. This should be considered a general warning for K-edge XMCD measurements, which probe the p orbital moment: a *zero* (within resolution) XMCD signal may hide residual spin magnetism. However, in our case, the fact that no reappearance of the K-edge XMCD signal occurred upon cooling supports the hypothesis of complete extinction of ferromagnetism. This would imply that the remaining hcp phase is also nonmagnetic at 0.69 of compression.

IV. CONCLUSIONS

We present here an extensive study on the structure and magnetism of cobalt under high-pressure and low-temperature conditions by XRD, K-edge XMCD, and supporting DFT calculations. This study was motivated by some gaps and incongruities in the literature in particular concerning the structural and magnetic state of Co at pressures above 130 GPa. We found that the equilibrium state at this very-high-compression condition is very sensitive to the pressurizing condition and presence of uniaxial stress. First, we provide an EoS for hcp cobalt up to around 160 GPa in quasihydrostatic conditions. The transition to the fcc structure is only observed under nonhydrostatic compression, pointing out the metastable character of these two phases. In nonhydrostatic conditions the hcp and fcc phases were found to coexist from $V/V_0 = 0.763$ to 0.694 , the maximum compression reached, where the hcp phase fraction was still 50%. A volume change of $\Delta V \approx 0.14 \text{ \AA}^3/\text{atom}$ (1.25%) was observed at the transition, in agreement with theoretical predictions. Interestingly, an inversion of the pressure derivative of the c/a ratio occurs in both quasihydrostatic and nonhydrostatic conditions starting at around $V/V_0 = 0.76$ and $V/V_0 = 0.78$, respectively. In the combined XRD-XMCD run we observe an inflection in the XMCD signal integral at this value of compression. Our results thus furnish the first experimental evidence that the inversion of the c/a pressure derivative is related to magnetism while is not related to the hcp-fcc structural transition. The K-edge XMCD signal is totally suppressed at $V/V_0 = 0.694$, in a mixed (50%) hcp-fcc phase. No reappearance of the XMCD signal occurred upon cooling down to 50 K. Assuming that the T_c does not fall below 50 K, our data thus indicate that the compression of cobalt to 150 GPa leads to a nonmagnetic state, characterized by zero local spin polarization. DFT calculations show that, as in the case of pure nickel, the K-edge XMCD is related to the $4p$ orbital moment rather than to the total spin moment, and

that the former gets suppressed more rapidly than the latter by the compression. The comparison to calculation supports that a nonmagnetic state is reached before the transformation to fcc is completed, i.e., the residual hcp phase is also nonmagnetic at $V/V_0 = 0.694$.

ACKNOWLEDGMENT

We acknowledge F. Wilhelm (ESRF) for fruitful discussions, P. Bouvier for help in the Raman measurements, and J. Jacobs (SESS-HP Pool, ESRF) for support in the DAC preparation.

-
- [1] V. F. Puentes, K. M. Krishnan, and A. P. Alivisatos, *Science* **291**, 2115 (2001).
- [2] V. A. de la Peña O'shea, P. Ramirez de la Piscina, N. Homs, G. Aromí, and J. L. G. Fierro, *Chem. Mater.* **21**, 5637 (2009).
- [3] V. A. de la Peña O'shea, J. M. Campos-Martin, and J. L. G. Fierro, *Catal. Commun.* **5**, 635 (2004).
- [4] C. S. Yoo, H. Cynn, P. Soderlind, and V. Iota, *Phys. Rev. Lett.* **84**, 4132 (2000).
- [5] F. Frey, W. Prandl, J. Schneider, C. Zeyen, and K. Ziebeck, *J. Phys. F* **9**, 603 (1979).
- [6] P. Modak, A. K. Verma, R. S. Rao, B. K. Godwal, and R. Jeanloz, *Phys. Rev. B* **74**, 012103 (2006).
- [7] J. E. Saal, S. Shang, Y. Wang, and Z. Liu, *J. Phys. Condens. Matter* **22**, 096006 (2010).
- [8] G. Steinle-Neumann, *Phys. Rev. B* **77**, 104109 (2008).
- [9] T. Jarlborg, *Physica C* **385**, 513 (2003).
- [10] D. Antonangeli, L. R. Benedetti, D. L. Farber, G. Steinle-Neumann, A. Auzende, J. Badro, M. Hanfland, and M. Krisch, *Appl. Phys. Lett.* **92**, 111911 (2008).
- [11] A. F. Goncharov, J. Crowhurst, and J. M. Zaug, *Phys. Rev. Lett.* **92**, 115502 (2004).
- [12] D. Antonangeli, M. Krisch, G. Fiquet, J. Badro, D. L. Farber, A. Bossak, and S. Merkel, *Phys. Rev. B* **72**, 134303 (2005).
- [13] Y. O. Kvashnin, W. Sun, I. Di Marco, and O. Eriksson, *Phys. Rev. B* **92**, 134422 (2015).
- [14] Y. S. Mohammed, Y. Yan, H. Wang, K. Li, and X. Du, *J. Magn. Mater.* **322**, 653 (2010).
- [15] G. Steinle-Neumann, L. Stixrude, and R. E. Cohen, *Phys. Rev. B* **60**, 791 (1999).
- [16] C. S. Yoo, P. Söderlind, and H. Cynn, *J. Phys. Condens. Matter* **10**, L311 (1998).
- [17] R. Torchio, A. Monza, F. Baudelet, S. Pascarelli, O. Mathon, E. Pugh, D. Antonangeli, and J. P. Itie, *Phys. Rev. B* **84**, 060403(R) (2011).
- [18] Bo Kong, Ti-Xian Zeng, Hong-Bin Xu, De-liang Chen, Zhu-Wen Zhou, and Zhi-Jian Fu, *Comput. Mater. Sci.* **104**, 130 (2015).
- [19] R. Torchio, Ph.D. thesis, Università degli Studi di ROMA TRE, Rome, Italy and Université Joseph Fourier, Grenoble, France, 2012.
- [20] V. Iota, J.-H. P. Klepeis, C.-S. Yoo, J. Lang, D. Haskel, and G. Srajer, *Appl. Phys. Lett.* **90**, 042505 (2007).
- [21] N. Ishimatsu, H. Maruyama, N. Kawamura, M. Suzuki, Y. Ohishi, and O. Shimomura, *J. Phys. Soc. Jpn.* **76**, 064703 (2007).
- [22] N. Ishimatsu, N. Kawamura, H. Maruyama, M. Mizumaki, T. Matsuoka, H. Yumoto, H. Ohashi, and M. Suzuki, *Phys. Rev. B* **83**, 180409(R) (2011).
- [23] R. Torchio, Y. O. Kvashnin, S. Pascarelli, O. Mathon, C. Marini, L. Genovese, P. Bruno, G. Garbarino, A. Dewaele, F. Occelli, and P. Loubeyre, *Phys. Rev. Lett.* **107**, 237202 (2011).
- [24] R. Le Toullec, J. P. Pinceaux, and P. Loubeyre, *High Pressure Res.* **1**, 77 (1988).
- [25] A. Dewaele, P. Loubeyre, and M. Mezouar, *Phys. Rev. B* **70**, 094112 (2004).
- [26] M. Mezouar, W. A. Crichton, S. Bauchau, F. Thurel, H. Witsch, F. Torrecillas, G. Blattmann, P. Marion, Y. Dabin, J. Chavanne, O. Hignette, C. Morawe, and C. Borel, *J. Synchrotron Radiat.* **12**, 659 (2005).
- [27] S. Pascarelli, O. Mathon, T. Mairs, I. Kantor, G. Agostini, C. Strohm, S. Pasternak, F. Perrin, G. Berruyer, P. Chappellet, C. Clavel, and C. M. Dominguez, *J. Synchrotron Radiat.* **23**, 353 (2016).
- [28] A. Dewaele, M. Torrent, P. Loubeyre, and M. Mezouar, *Phys. Rev. B* **78**, 104102 (2008).
- [29] P. Vinet, J. Ferrante, J. Rose, and J. Smith, *J. Geophys. Res.* **92**, 9319 (1987).
- [30] D. Errandonea, Y. Meng, M. Somayazulu, and D. Hausermann, *Physica B* **355**, 116 (2005).
- [31] A. Dewaele, V. Stutzmann, J. Bouchet, F. Bottin, F. Occelli, and M. Mezouar, *Phys. Rev. B* **91**, 134108 (2015).
- [32] H. K. Mao, J. Xu, and P. M. Bell, *J. Geophys. Res.* **91**, 4673 (1986).
- [33] N. C. Holmes, J. A. Moriarty, G. R. Gathers, and W. J. Nellis, *J. Appl. Phys.* **66**, 2962 (1989).
- [34] H. Cynn and C. S. Yoo, *Phys. Rev. B* **59**, 8526 (1999).
- [35] H. Fujihisa and K. Takemura, *Phys. Rev. B* **54**, 5 (1996).
- [36] P. Lazor, Ph.D. thesis, Uppsala University, 1994.
- [37] P. Blaha, K. Schwarz, G. Madsen, D. Kvasnicka, and J. Luitz, *WIEN2k*, An Augmented Plane Wave + Local Orbitals Program for Calculating Crystal Properties (Karlheinz Schwarz, Techn. Universität Wien, Austria, 2001).
- [38] J. P. Perdew, K. Burke, and M. Ernzerhof, *Phys. Rev. Lett.* **77**, 3865 (1996).
- [39] O. Eriksson, B. Johansson, R. C. Albers, A. M. Boring, and M. S. S. Brooks, *Phys. Rev. B* **42**, 2707 (1990).
- [40] C. T. Chen, Y. U. Idzerda, H.-J. Lin, N. V. Smith, G. Meigs, E. Chaban, G. H. Ho, E. Pellegrin, and F. Sette, *Phys. Rev. Lett.* **75**, 152 (1995).
- [41] J. Stohr and H. Siegmann, *Magnetism: From Fundamentals to Nanoscale Dynamics*, Springer Series in Solid-State (Springer, Berlin, 2006).
- [42] S. Chadov, J. Minr, M. I. Katsnelson, H. Ebert, D. Kideritsh, and A. I. Lichtenstein, *Europhys. Lett.* **82**, 37001 (2008).